Paper 24

Deep Exploration with EM in Boreholes

Lamontagne, Y. [1]

_____
1. Lamontagne Geophysics Ltd., Kingston, Ontario, Canada

ABSTRACT

BHEM has become an essential tool in the deep exploration for massive sulphide deposits. BHEM measurements can be used to search around boreholes for off-hole conductors or to define the extent of in-hole conductors. The measurements are made using a large surface transmitter loop and a down-hole probe string which consists of the EM sensor and orientation tools. Most currently used BHEM sensors either use the induction coil or field feedback induction coil designs but fluxgate magnetometer BHEM sensors have recently been introduced. The deep BHEM systems are time domain systems using either a "castle" or ramp waveform. The practical ramp waveform system now uses a highly modified ramp waveform and deconvolution techniques to produce a square wave system response, the periodic approximation of the step response. With the castle waveform systems, off-time measurements are not sensitive to very long decay responses. Approximate step calculations are used to resolve these responses. With the use of noise reduction techniques and more powerful transmitters, BHEM measurements are now routinely done over a frequency range more than an order of magnitude lower than a decade ago in the search for very conductive targets in complex conductive environments. Recent deep BHEM discoveries range from simple off-hole target detection to the careful persistent application of BHEM techniques in complex environments.

INTRODUCTION

Over the last ten years, electromagnetic measurements in boreholes (BHEM) have taken an ever increasing role in deep mineral exploration. Ten years ago, BHEM was already established as a standard exploration tool and in some instances drilling programs were configured specifically to take advantage of BHEM capabilities.

This approach has now become almost generalised in deep exploration programs and in some areas the whole exploration strategy is relying on the expanding capabilities of BHEM techniques.

So, while the last decade have been a period of consolidation and incremental improvements on the technology side, perhaps the greatest progress has been in the increasing confidence in its application to deep exploration problems which has resulted in numerous mineral discoveries.

WHY USE DEEP HOLE BHEM?

In contrast to borehole logging measurements which characterise in more detail the rocks intersected by the hole, the main purpos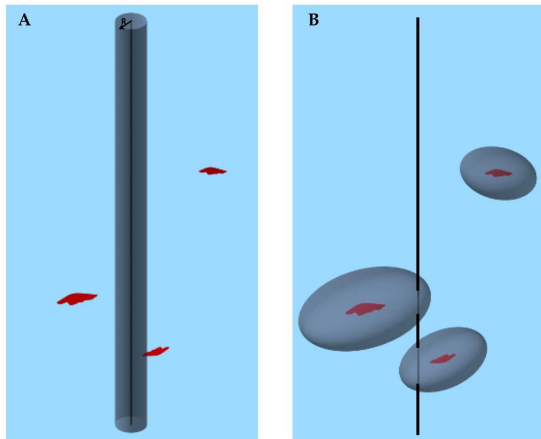e of borehole EM measurements is to explore around boreholes. BHEM uses boreholes as geophysical survey lines to look around boreholes in the same way that surface EM techniques uses surface measurements to look for conductors at depth. The specific purpose of BHEM in most applications is to detect, locate and characterise conductors and its main application is in massive sulphide exploration.

The effect of BHEM has been described as an increase in the effective diameter of the hole for the purpose of massive sulphide detection as depicted in Figure 1A. Considering a volume with a sparse distribution of deposits of a typical size, the radius of investigation is thought to be increased from the radius of the hole up to several hundred metres as depicted in Figure 1A. Since the distance of detection of a good conductor depends mainly on its size, the uniformly increased hole diameter view is incorrect.

A more accurate visualisation is that BHEM measurements increase the effective detection distance of deposits in proportion to their size and electrical properties as depicted in Figure 1B. It is as if conductive targets acquired a halo increasing their detection volume considerably. This halo could be defined more quantitatively in terms of the expected anomaly amplitude as a function of distance. As technology improves, the detection halo around conductive targets extends to greater distances in proportion to their size. This analogy is oversimplified as it does not take into account the presence of man made noise and interfering responses, but it has some merit

in showing the value of deep BHEM in exploring at depths well beyond surface detection.

The attractiveness for BHEM measurements is that for a small fraction of the drilling costs, the volume of detectability of prospective targets can increase by a factor of up to one thousand or so in favourable low noise cases and by still a large factor in less favourable near-mine exploration situations. This advantage is maximised in deeper (i.e. longer) holes in which long wavelength anomalies can be well defined.
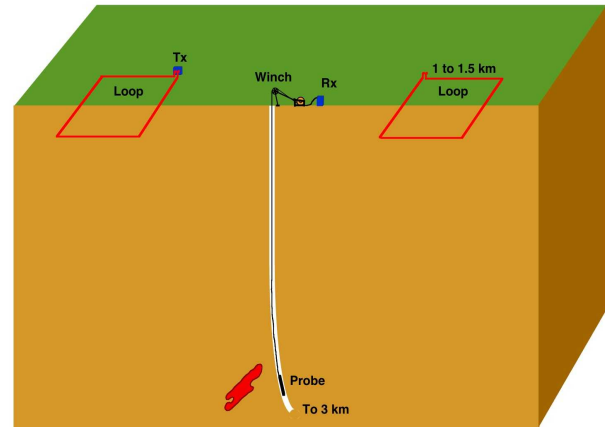

Figure 1: BHEM measurements can detect the response of conductors up to some distance from the borehole. The detection distance is not constant as depicted in A. It is mainly proportional to the size of each conductor as shown in B.

DEEP BHEM APPARATUS & CONFIGURATION

BHEM refers to geophysical techniques methods which measure the inductive earth response to time varying magnetic fields excited by a transmitter antenna. The configuration used in deep BHEM exploration is illustrated in Figure 2. The measurements are usually made at stations down a hole by a sensor linked to a surface receiver apparatus.   In deep exploration, the transmitter configuration consists of a large surface transmitter wire loop normally greater than 1 km square into which current of a particular waveform is injected by a transmitter apparatus powered by a motor generator. For holes deeper than 2000m, the transmitter loop size tends to be greater, being typically 1500x1500m in size.

The sensor is attached to a data cable of special construction that can either be a multiwire or fibre-optic cable. It is lowered down the hole by means of a winch and cable spool system with electrical slip ring connection to the receiver input cable. The down-hole probe consists of the EM sensor which can measure one, two or three components and other modules depending on the type of measurements.

All current systems effectively perform 3-axis magnetic field measurements either using a single pass three-axis EM tool or using two passes, one with an axial component tool and the other with a two-axis transverse component sensor. Photographs of typical field setups at borehole sites are shown in Figure 3.
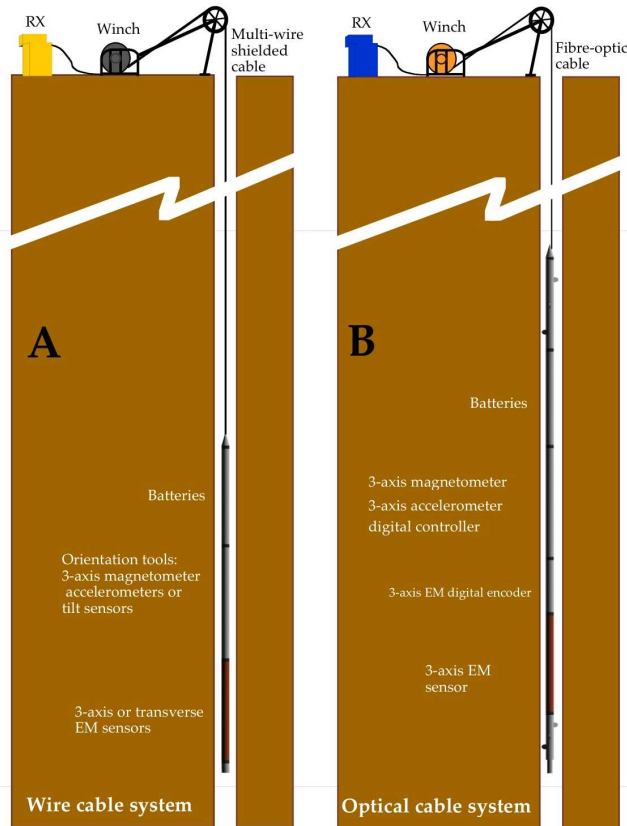

Figure 2: Typical deep BHEM configuration. Two or more transmitter loop locations are needed to insure good primary field coupling if the strike and dip directions of the target conductors are unknown.

Figure 3: Photos of typical BHEM setups at the borehole collar. On the left is the setup of the Geonics BH-43-3 BHEM system with the assembled down-hole string held vertically out of the hole and winch. The receiver is in the foreground. On the right is shown the BHUTEM4 system comprising the winch system, receiver and the assembled probe string lying on the ground.

Two typical receiver/sensor setups are sketched in Figure 4. In one system (A), the downhole package consists of the sensor, orientation tools, and a battery module. It is linked to the surface by a multi-wire shielded cable spooled by a winch. Slip ring contactors mounted on the axis of the spool connect the downhole cable to the receiver data cable. The receiver samples the data digitally, and processes them into channel averaged data which are then stacked, reduced and stored for later retrieval. The downhole probe can be a 3-axis sensor, a two-axis transverse component sensor or an axial component sensor (without orientation tools) depending on the configuration.

_____

Figure 4: Typical BHEM downhole and collar configurations for BHEM systems. In configuration A, the data cable is a shielded multiwire cable and the down-hole probe has analogue outputs. In B, a fibre-optic data cable is used, and digital encoding takes place down the hole.

In configuration B, the down-hole data are sent from the down-hole package to the surface through a fibre-optic cable. This requires that the analog-to-digital conversion of the EM and orientation tool data be done downhole and encoded for serial transmission. In the BHUTEM4 implementation (sketched), motion wheels are used to remotely signal the downhole system from the surface. The fibre optic cable is terminated at the free end by an optical transmitter and at the inner spool end by an optical receiver connected electrically to the slip ring contactor.

BHEM SENSORS

The heart of the BHEM system is the sensor that measures the EM response. In this respect, the main technology leap in the decade before 1997 could be effectively described with three words: three axis measurements. In the last decade, the progress has been on several fronts. The two main trends have been towards "on" time measurements and towards lower frequencies of operation. These trends led to the main BHEM instrumentation and data processing developments in the period.

There are 3 types of BHEM sensors currently in use. These are induction coil sensors, field feedback induction coil sensors, and the recently introduced flux-gate magnet-ometer sensors.

An induction coil sensor as sketched in Figure 5A is a direct application of Faraday's law.

$$Emf = -df/dt$$

Multiple turns of wire sense any time variations of the magnetic flux linking the windings. Because of the diameter restriction of a borehole sensor, a core of magnetic material such as ferrite is necessary to concentrate the flux in the windings. The signal is amplified and then conditioned for tranmitting up the cable to the receiver.

The effective flux F in the sensor is related to the ambient H field in the hole through the core cross-sectional area A, the core factor f, and the number of turns N:

$$B_c = F\mu_0 H_c$$
$$F = N\ A\ B_c$$

where H_c is the component of the magnetic field H measured, and μ_0 is the magnetic permeability of free space. The core factor f is dependent on the shape and magnetic permeability of the core.

The effective area Ae is often used to define the low frequency detection gain of an induction sensor. Ae is the area of the single turn "air cored" loop with the same low frequency detection gain. This is to be contrasted to the sensitivity which is conventionally defined as the noise density of the sensor as a function of frequency.

Using Ae, the above relationships can be rearranged as:

$$Ae = f\ N\ A$$
$$Emf = Ae\ \mu_0\ dH_c/dt$$

The simple relationships hide many complexities in the design which result in a trade-off between bandwidth, effective area and sensitivity. Two commercial examples of induction coils are the Crone 3D-PEM system and the Geonics BH43-3 systems.

A *field feedback induction sensor* uses an induction coil sensor as a null detector using feedback windings to cancel out the time varying field as illustrated in Figure 5B. In such a system, the current that is fed back to cancel the field is a measure of the field. The feedback windings are arranged in such a fashion that the field that they produce is uniform over the induction coil sensor. In the case of the axial sensor depicted, this is achieved by using feedback windings arranged as a long solenoid which would produce an almost perfectly uniform H field provided that the spacing E is small relative to the diameter of the sensor. In this case the uniform field produced inside the solenoid with a current I is simply:
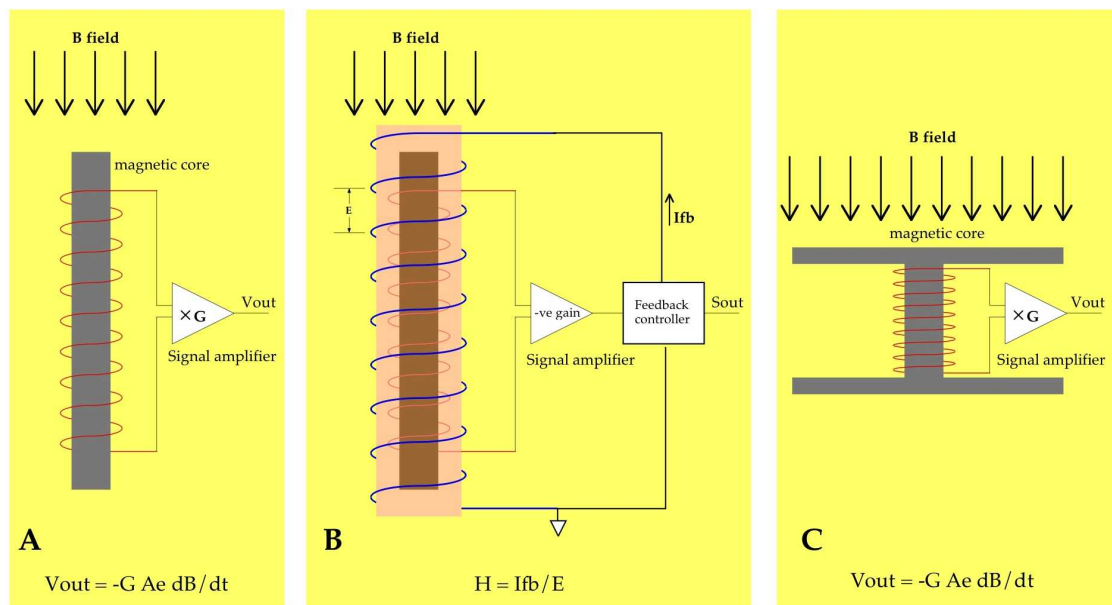
$$H = I/E$$

While the induction coil sensor makes use of Faraday's law to define its detection gain, the field feedback sensor makes use of Ampere's law. A field feedback sensor requires additional circuitry to control the feedback. In spite of its greater

_____

complexity, the field feedback sensor can have advantages in situations where extreme gain, stability and signal fidelity are required. The field feedback also makes it possible to tailor the frequency response of the sensor up to the bandwidth limit of the feedback system. If suitable feedback stability is achieved, the noise sensitivity of field feedback sensor is dependent on the characteristics of the embedded induction coil sensor and its pre-amplifier, as it is for the induction coil sensor. So for a field feedback induction coil, the design trade-off between bandwidth and sensitivity is the same as for a conventional induction coil.

A commercial example of a field feedback induction coil sensor is the BHUTEM4 sensor, a three component field feedback sensor in which the analog to digital conversion is part of the feedback circuitry. The digital outputs are numerical measures of the components of DH, the difference in the H field at the 10μs sampling interval.

Figures 5A and 5B illustrate the basic configuration of axial component sensors featuring a long core to channel the magnetic flux. In a transverse component sensor depicted in Figure 5C, the shape of the core is changed to capture the transverse component of the field along the length of the sensor and channel it through the windings.

A new type of BHEM sensor using a low noise three-axis *flux-gate magnetometer* has recently been introduced by several manufacturers. Many types of flux-gate sensor design would be suitable for this type of application, including three independent flux-gate sensors or for example the single cubic Develco type three-axis ringcore sensor. The raw measurements from a flux-gate sensor have a poor intrinsic linearity which would result in a dependence of the sensor gain on the DC magnetic field. So all modern flux-gate magnetometers use field feedback, where the cancelling field is fed back and used as the measure of the field, much as in the field feedback induction coil sensor.

Figure 5: Schematic representations of different types of sensors commonly used in BHEM systems. A shows a simplified induction sensor with a magnetic core to increase the magnetic flux density in the pickup windings. In B, a field feedback induction sensor is depicted. The feedback current is a direct measure of the B field within the bandwidth of the sensor. The output Sout may be proportional to B or dB/dt depending on the controller circuitry. For use as a transverse sensor, the magnetic core shape is modified to capture the transverse magnetic flux over the length of the sensor as shown in C.

ORIENTATION TOOLS

In orienting and locating the down-hole measurements, it is assumed that the sensor lies at the end of the cable along the hole trajectory which can be reconstructed from the dip and azimuth measurements which are normally obtained from a down-hole gyroscopic survey. The depth of the probe along the hole is measured by means of an encoder mounted on a depth wheel. Using the depth and borehole trajectory data, the coordinates of the sensor stations (x,y,z) and the direction of the axial component of the sensor can be calculated for each survey station.
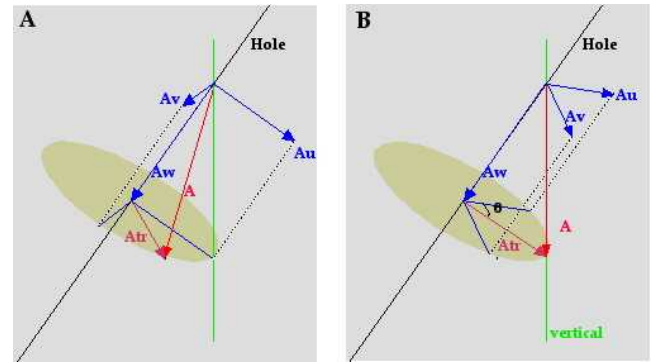
To orient the transverse components, the roll angle of the sensor must be determined. A number of tools can be used to do this. They are all based on basically the same principle, that of comparing the direction of a measured vector field to its calculated direction and of finding the roll angle of the sensor that gives the closest match. The three fields used for this purpose are the EM field itself, the earth's magnetic field, and the gravity field. Since the direction of the total EM field can be strongly affected in the presence of EM anomalies, this method of orientation has been mostly abandoned over the last fifteen years. The main orientation tools currently used are accelerometers, tilt sensors, and magnetometers.

_____

Figure 6 shows how the roll angle q is determined in the case of accelerometer measurements. Measurements of the EM sensors and the orientation tools are made on three the orthogonal axes attached to the sensor. Figure 6A shows the acceleration vector A assuming a roll angle of zero and the direction of the vertical gravity field vector. In Figure 6B the probe is rotated around its axis to align the measured acceleration to its closest approach to the vertical field. The roll angle q is determined by this fit.
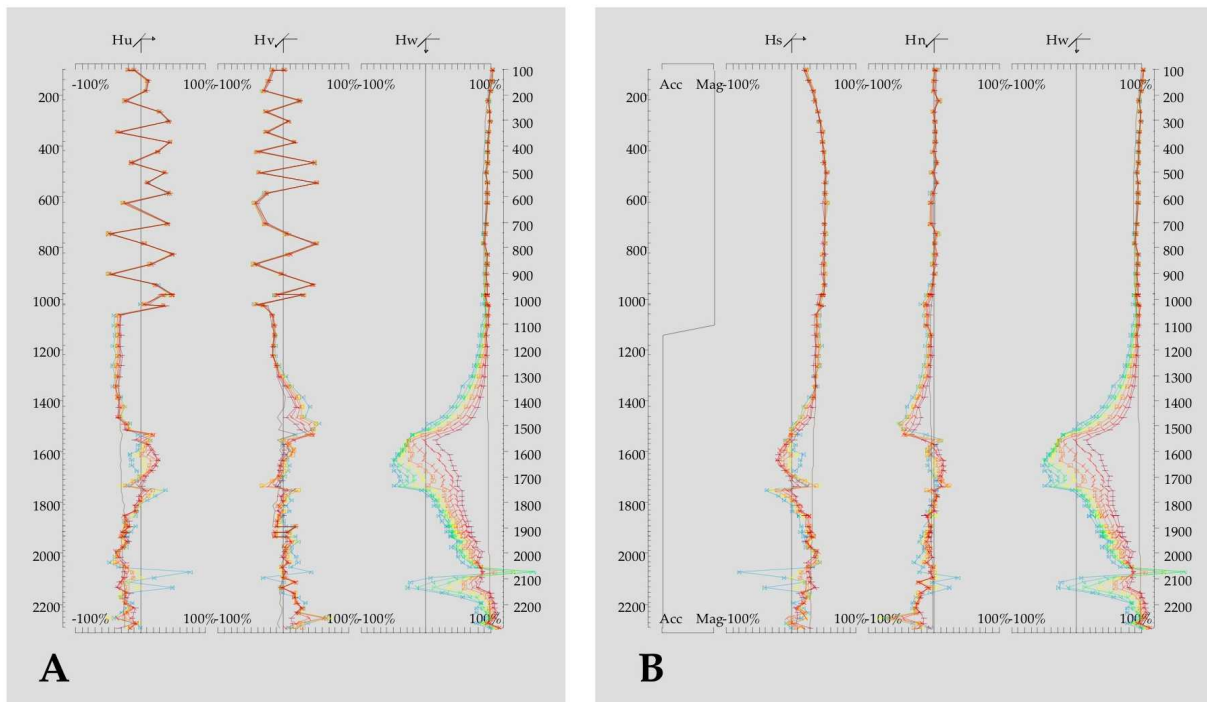
Unoriented data are shown in Figure 7A. The EM field components in u and v, the raw transverse components have jumps where the probe in the hole rolls between stations. When the roll angle is determined at each station, the u and v orientations in space can be determined, and the field can be calculated in any desired orientation. In Figure 7B, the transverse EM data are resolved into the s and n directions in and normal to a chosen reference drill section plane, revealing a single anomaly. Once the data are oriented into components pointing in known directions in space, the measured anomalies can be interpreted in terms of target conductors located in a known direction with respect to the borehole.

The convention used for oriented components vary from system to system as shown in Table 1. If the section azimuth is chosen as the hole azimuth than the equivalence is as given in the table.

Figure 6: An accelerometer orientation tool measures the three components of the gravity field in the raw directions of the sensor u,v,w shown in A assuming a zero roll angle. In B, the u and v axes are rotated by an angle q such that the total acceleration vector A is made vertical. q is the roll angle

Figure 7: Three axis BHEM data before and after orientation. In A, the data of the raw sensor axes are plotted in total field format normalized to the primary field amplitude. In the top part of the hole where it is nearly vertical, the probe is rotating between stations. In the bottom part, the probe is hardly rotating but it is misoriented. The data in B were oriented using the magnetometer tool in the top part and the accelerometer tool in the bottom part.

Orientation errors

Each orientation tool fails when the field they measure is along the hole axis, and their performance is degraded when it is within a small angle of it. Such is the case for the accelerometer or tilt sensor tools in nearly vertical holes. For a hole at an angle gamma from the vertical, the expected orientation error E (in degrees) is related to the accelerometer error alpha in percent

_____

and to the angular error in the alignment of the probe axis in the hole beta by the relations:

$$A = \arcsin[(\sin(beta)+0.01*alpha)/\sin(gamma)]$$

then

$$
\begin{aligned}
E &\approx A && | \quad A < 90° \\
E &\text{ undetermined} && | \quad A \geq 90°
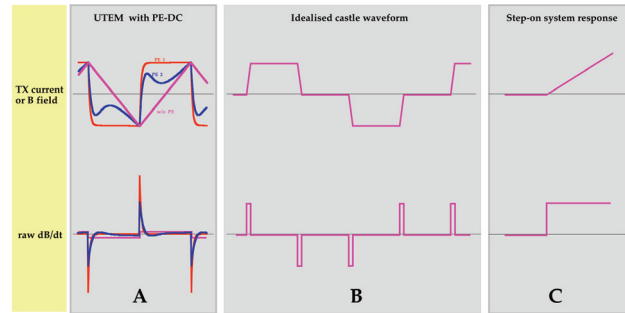\end{aligned}
$$

Table 1: Equivalence of oriented axis conventions for various BHEM systems. In BHUTEM4, the oriented axes are relative to a reference section. In other systems, the axes are relative to the hole azimuth. In the sketches it is assumed that the section azimuth and hole azimuth are the same.

System	Axial	Transverse in plane	Transverse normal	Axes
Boliden BHEM-99	X down	Z	Y	
Crone Pulse EM	Z up	X	Y	
EMIT Atlantis	A down	U	V	
Geonics BH43-3	Z up	X	Y	
LGL BHUTEM4	w down	s	n	

For example, for a hole dipping at 85°, if the raw precision of the accelerometers was 1%, the best achievable accuracy in the orientation would be 7° even with the probe was perfectly aligned in the hole and the hole trajectory perfectly known. For a hole dip of 89°, the best orientation error would be 36°, or a range of direction of 72°. With careful calibration and temperature compensation of orientation tools, their effective raw precision can be improved to a fraction of 1%.With these refinements, beta the sum of the hole orientation error (from the gyro data) and the probe alignment error is the main limitation in the achievable orientation precision in near vertical holes. This alignment error tends to be worse in absolute terms for near vertical holes where the probe tends to stick to the hole walls or where it may be free hanging. If the beta error was 1°, even with perfect accelerometer data, the orientation error for 85° dip would be 12°, and it would be basically undefined for holes steeper than 88°.

With an accelerometer or tilt tool based orientation tools, reliably oriented data can be obtained only for gyro surveyed holes dipping at 85° or less. For the magnetometer orientation tool, the reference orientation is that of the local earth's total magnetic field instead of the vertical. Although its performance is affected by magnetic anomalies, it is the preferred orientation tool in near vertical holes or in holes without azimuthal information.

In systems with redundant tools, the data reduction software can typically calculate the oriented data for either tool or with a weighted fit of both sets of tools.

Figure 8: System waveforms for (A) the UTEM system, (B) castle waveform systems, and (C) the ideal step-on system response. The transmitter current waveforms have the same shape the primary B field that would be measured by a magnetometer. The raw dB/dt waveforms show the primary signal seen by an induction coil. The UTEM waveforms are for no pre-emphasis (purple), a first order pre-emphasis filter (red), and a second order one (blue).

WAVEFORMS & TRANSFORMATIONS

The current commercial BHEM system are all time domain systems (TDEM). The only frequency domain system in use is the Boliden BHEM-99 system, a three-axis BHEM system measuring phase and amplitude. The two main TDEM waveform types used in these systems have remained generally the same for thirty years: the BHUTEM system using a conceptual ramp waveform (Figure 8A) to measure the square wave response closely related to the step response, and the other systems such as Pulse EM using a "castle" waveform (Figure 8B) to measure a response resembling the impulse response. In some implementations of the castle waveform the turn-off ramp is controlled to be a linear slope (Crone Pulse EM), whereas in others, the turn-off is exponential or uncontrolled. The turn-on current slope is usually of roughly exponential in shape. It will be assumed in the following that both turn-on and turn-off slopes can be represented with constant slopes, which makes little difference in the main features of the responses.

There has been a significant evolution in recent years in both types of waveforms. Comparative measurements of the two types of waveforms in high conductivity target detection at the deep Victor discovery and at Voisey's Bay confirmed the poor sensitivity of off-time castle waveform measurements to real life highly conductive targets. Approximate step response calculations from Pulse EM measurements (Frazer 1994, Ravenhurst 1998, Smith and Balch 1998) were then introduced and are now used routinely. The Frazer transformation assumes that the turn-off current slope is constant whereas the Smith and Balch calculation achieves similar results for an uncontrolled turn-of. If the switch-off ramp time is W the step response F is calculated from the pulse data P using the formula:

$$F(t) = F(t-W) + P(t)$$

over the sampling range S starting at the beginning of the turn-off ramp.

_____

The aim of these transformations is to provide an approximate estimate of the step-on response (Figure 8C) which is desirable in the detection of highly conductive targets.
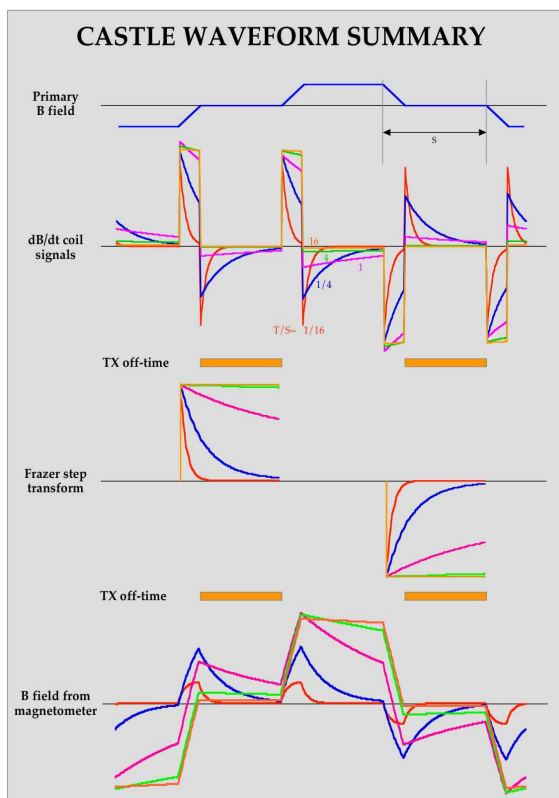
In the UTEM system, the use of the pre-emphasis-deconvolution (PE-DC) signal noise rejection technique (Macnae et al., 1984) has evolved to very high level of enhancements in new transmitters through the use of digital waveform synthesis (Figure 8A). This was particularly necessary in using ramp waveforms at low frequencies to counter the diminishing signal levels as the rate of change of the waveform is decreased. The aim of this technique to use a linear filter to emphasise the transmitted field strength in the bands of frequencies where the signal to noise is poor such that the inverse (deconvolution) filter can reduce the noise in these bands without distorting the system response.

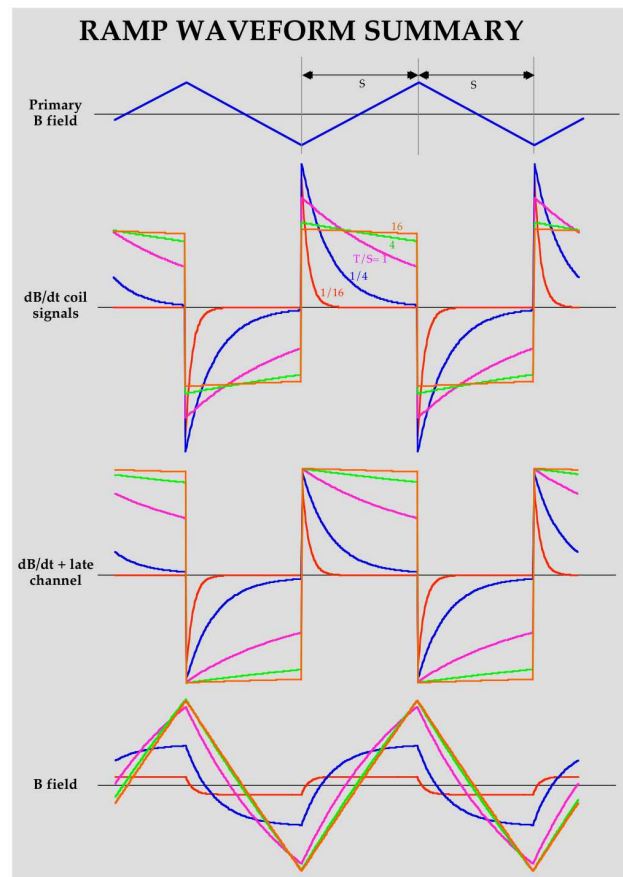Another trend in surface and airborne EM measurements and now with down-hole flux-gate sensors has been towards direct B field measurements which may be advantageous from a signal-to-noise point of view for measurements at very low frequencies.

Figures 9 and 10 give summaries of the responses seen by each system for exponential responses of five decay times ranging from a sixteenth to sixteen times the sampling time.

For the castle transmitter current waveform (Figure 9), the raw response as seen with an induction coil has high amplitudes during the current turn-on and turn-off ramps and the two longest decay responses vanish in the off-time. In the Frazer transformed data, the two longest decay responses show up as large undecaying responses. The magnetometer data responses are untransformed and are shown both during the on-time and off-time, although channel sampling is usually confined to the off-time.

Figure 9: Summary of waveforms for "castle waveform" systems. The response waveforms are for five exponential decay responses with ratio of decay time T to sampling range S of 1/16 (red), 1/4 (blue), 1 (purple), 4 (green) , 16 (orange). All system responses are sensitive to moderate decay time responses (blue, purple). The coil and Frazer step are both sensitive to short decay responses, but of these responses the Frazer step alone is sensitive to long decay responses (green, orange). The magnetometer is poorly sensitive to short decay responses. In the off-time, it is more sensitive to moderately long decays than the dB/dt response, but it is insensitive to very long decays (orange). In the on-time, the magnetometer is sensitive to very long decay and has better discrimination of long decays (green vs orange).

Figure 10: Summary of waveforms for the ramp waveform. The response waveforms are for five exponential decay responses with ratio of decay time T to sampling range S of 1/16 (red), 1/4 (blue), 1 (purple), 4 (green) , 16 (orange). This is the UTEM system response after deconvolution. The dB/dt waveform is sensitive to all decay times but the initial response is up to two times greater for shorter decay. Adding the late channel response to each half-cycle gives an approximate step response with equal initial response. The B field response has the same shape as the causative induced current in the conductors.

Figure 10 shows the responses for a ramp current waveform which would give a square wave system response. A rough step transformation is obtained by adding the late channel response to each half-cycle. This eliminates the 50% attenuation of the initial amplitude of very long decay seen in the raw dB/dt signals.

The square wave response, and the Frazer step calculation or on-time magnetometer response are all capable of detecting conductors with very long and even infinite decays as is the ideal step-on response. The magnetometer off-time response is more sensitive to long decay responses than the raw off-time pulse data. However, in contrast to the various step approximations, it is not sensitive to targets of decay times much longer than the sampling range.

LOW FREQUENCY MEASUREMENTS

BHEM measurements are being made to increasingly long sampling times. Ten or fifteen years ago, measurements at base frequencies below 10Hz were relatively rare. The usual base frequencies were most often around 25 or 30Hz with sampling gates limited to a range of less 20ms. The sampling range has now been extended to one second or more on some systems and a majority of the measurements are done with sampling ranges exceeding 100ms. The main reason for this development is the increasing use of BHEM in the search for highly conductive massive sulphides in electrically complex environments affected by the interfering responses of conductive rock units or more commonly of extensive low-grade mineralisation.
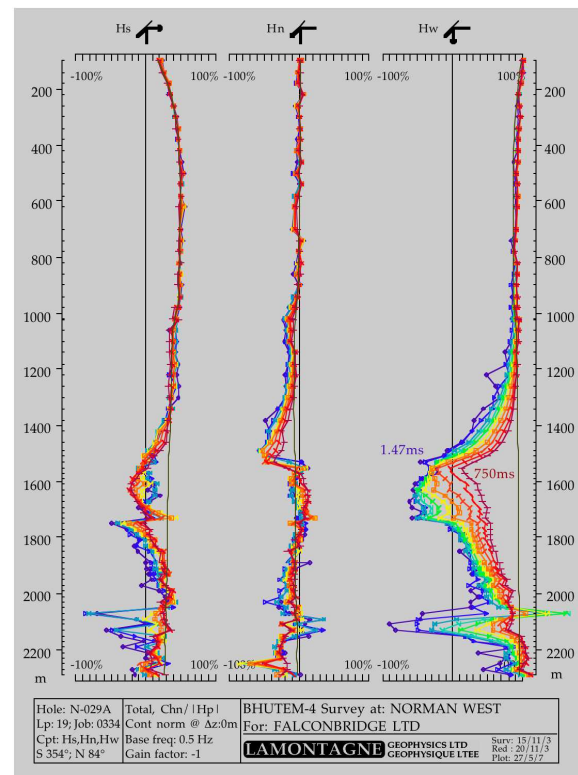
Measurements at lower frequencies are intrinsically more difficult to do because there are fewer transients to average in a given stacking period. The progress towards this goal has been achieved through the combination of several factors:

1. Higher power, more effective transmitters and larger transmitter loops
2. More advanced noise rejection processing such as PE/DC, optimised stacking algorithms, and channel window shapes
3. Frequency interleaving for common cultural noise sources
4. Sensor refinements to improve low frequency fidelity
5. Longer stacking times

Figure 11 shows a data example which is currently near the noise limit for deep low frequency measurements. These data, at a 0.5 Hz base frequency (1s sampling range), were acquired to 2.3km depth in the Sudbury area using a transmitter loop of 2km size over a three day period including a period of experimentation to optimise the survey parameters. In this particular instance, the use of tapered channel windows rather than the standard boxcar windows made a significant difference in the data quality, likely because of its better rejection of power line noise. We see a greater data scatter at depth in spite of longer stacking times which ranged from 3.0 to 12.8 minutes.

The data are presented in total field three-axis format normalised to the primary field strength, where anomalies are the difference between the channel data profiles and the calculated primary field curves for each component. The distracting local anomalies disappear by the last two channels

and we see that the main anomaly at 1600m depth (in-hole) has a decay time well in excess of one second. Referring to the component direction arrows at the top of the profile, the centre of the main in-hole zone was interpreted to be in the -n direction and the zone is dipping in the -s direction. This main anomaly is due to a large accumulation of uneconomic sub-layer sulphides. In doing the low frequency measurements, it was hoped that the response of this large zone would decay to the point where it would be possible to look for other targets to some distance around the hole. The results indicate that the frequency would need to be reduced below 0.1 Hz to achieve this.
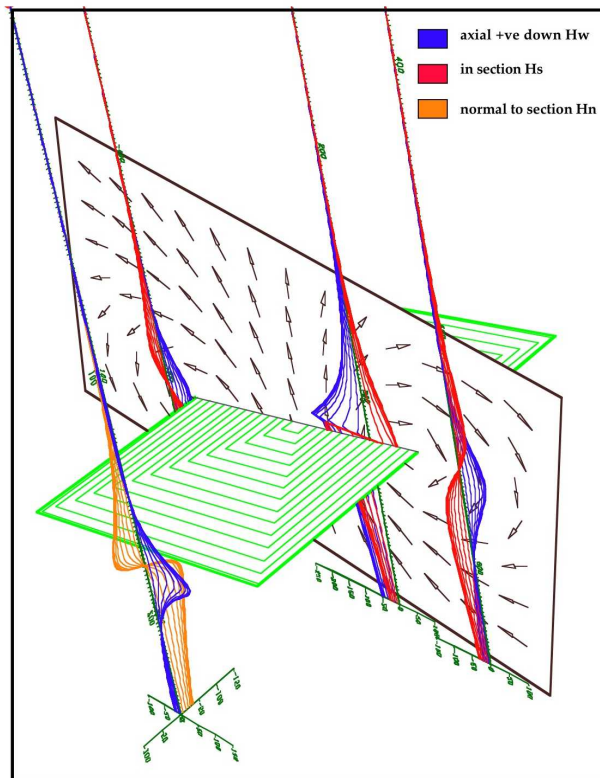

Figure 11: Example of low frequency data. Data measured at 0.5Hz to 2300m depth. Late channel precision is improved through the use of tapered channel windows, but this increases early channel scatter.

TYPICAL ANOMALY SHAPES

The responses observed in BHEM data can take a wide variety of shapes and patterns in the oriented 3-axis data. Figure 12 shows a few typical simple anomaly shapes for one "in-hole" and three "off-hole" anomalies. An off-hole anomaly occurs when the borehole or the continuation of the borehole misses the target conductor. The most recognizable feature of an off-hole anomaly is usually its smoothness. For in-hole anomalies, there are often sharp discontinuities in some or all components. When plotted in total rather than secondary field format an on-time or step response off-hole anomaly shows an overall increase in the total field whereas there is an overall attenuation of the total field amplitude in an in-hole anomaly.

Anomaly shapes are simplest when the plane of a tabular conductor is normal to the hole axis as in Figure 12. Dipping and plunging conductors have anomalies with the most complex anomaly shapes and usually little or no symmetry. Off centre in-hole anomalies have more complex shapes with abrupt jumps on one or more components where there is induced current flowing at the point of intersection.

The interpretation of conductor location and orientation is based on the field vector directions which vary along the hole. These indicate that the field is either curving around conductor edges or diverging away from the centre of a broadside conductor. For an in-hole response, the direction to the nearest edge can be defined by comparing the polarity of the jump in the tangential field to that of the normal incident field. The location and distance of off-hole conductors can normally be determined by means of 3-axis data with the notable exception of the coplanar conductor where the symmetry of the conductor with respect to the hole makes the interpretation ambiguous.

Figure 12: Simple BHEM anomaly shapes for four holes located on the principal axes of a conductor. The directions of the secondary field can be inferred by the BHEM axial and transverse component anomalies.

TECHNICAL CHALLENGES OF DEEP BHEM

Deep BHEM measurements present many more difficulties than advantages when compared to surface EM measurements. There are few advantages to doing EM measurements downhole except:

1- normally there is no motional noise which can be a serious problem for both surface EM (due to wind) or airborne EM measurements
2- reduced high frequency and powerline noise in some very deep holes

The difficulties of deep BHEM surveys are many, but I have singled out the main ones affecting deep BHEM exploration.

BHEM problems in general:
1- the geometrical fall-off of the primary field with depth
2- the large dynamic range of signals over space and time
3- the limited diameter of the sensors
4- the harsh physical conditions encountered in deep boreholes
5- the uncertainty in the hole trajectory data
6- hole blockage and probe loss problems

Other problems in near mine areas:
7- the high levels of cultural EM noise
8- logistical difficulties in transmitter loop placement
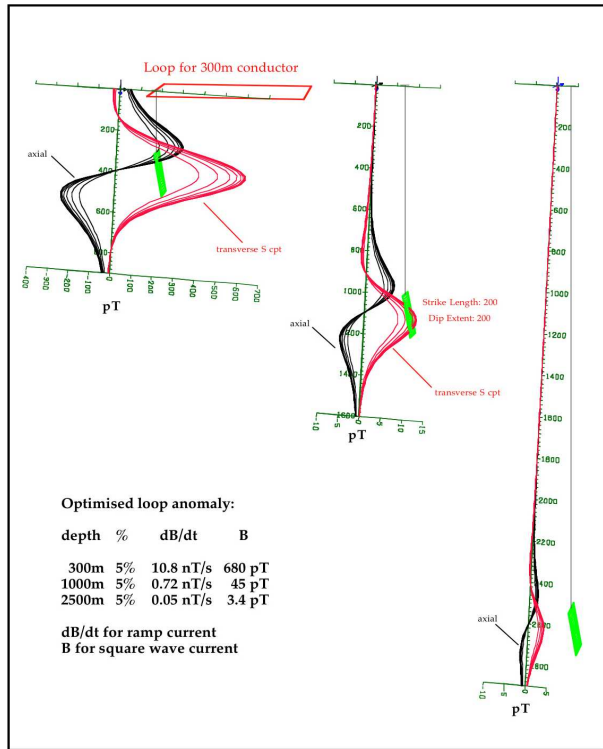9- regulatory constraints of industrial environment

This list shows that the technological challenge of deep BHEM measurements is a topic in itself. The detection of deep small amplitude and the dynamic range encountered in BHEM are issues of particular interest.

SIGNAL STRENGTH & DYNAMIC RANGE

The signal amplitudes and dynamic ranges seen in deep BHEM measurements are of the same magnitude as they would be in large loop surface EM measurements extending to several kilometres outside the loop.

To get an idea of the absolute anomaly amplitudes seen in BHEM one can experiment with modelling software as shown in Figure 13. It is a composite picture of three models showing the amplitude of anomalies produced by excellent conductors of the same size (200m) and distance from the hole (also 200m) at three depths of 300m, 1000m and 2500m along a borehole. In each case, the transmitter loop has a peak dipole moment of 20 million $A.m^2$, typical of what is used in deep BHEM measurements. The size and location of the transmitter loops were optimised to produce the largest response in absolute terms in each case. The curves show the B field response for a square waveform in pT and a summary table shows also the peak-to-peak amplitudes for the dB/dt ramp response waveform. The maximum peak-to-peak inductive limit anomaly as a percentage of the primary field is roughly the same (5%) for all three cases.

The dB/dt and B peak-to-peak responses of the deep conductor in this case would be 0.05nT/s and 3.5pT. Normalised to transmitter current, it would be 0.34 pT/A. In low noise conditions, such as for example a remote location in Labrador, an anomaly of this size would be readily detectable in both the axial and transverse components data. In noisy conditions typical to mining areas, its detectability may however be marginal.

_____

Figure 13: Anomaly amplitudes for three conductors of the same size and distance to hole at three different depths. The transmitter dipole moment was constant, but the loop size and location were optimised in each case to give the largest anomalies.

The geometrical fall-off in the anomaly amplitudes in these three models is 200:1 (680pT to 3.4pT) and since the primary fields are twenty times greater than the anomalous responses, the deep anomaly is 4000 times smaller than the primary field at 300m depth. Depending on the loop position a small resolvable anomaly can easily be more than 10,000 smaller than the maximum rms primary field in the hole near the surface. With dB/dt measurements, the dynamic range may be further increased by orders of magnitude depending on the decay time of the response and the waveform shape.

To mitigate this extreme signal strength range, loop size and positions can be designed to reduce the dynamic range, and stacking time increased for deeper measurement stations. In low noise environments, the use of more sensitive sensors, longer stacking times or a higher transmitter output can all help in the resolution of small deep anomalies whereas in noisy near mine environments ambient noise often dominates the signal and only higher transmitter output or longer stacking times are of any help.

PROBE SIZE & SENSOR SENSITIVITY

The probe diameter is a strong limiting constraint that limits the low frequency sensitivity of BHEM sensors in general, and more critically so for the transverse components. This would affect the performance of these tools in situations of moderate noise where the low frequency resolution of the measurements may be limited by the intrinsic sensor noise rather than external noise. While the axial sensitivity is strongly affected by the sensor length, the transverse sensitivity is more strongly dependent on the probe diameter. Both axial and transverse sensitivities improve with sensor size, particularly at low frequency. As an illustration, Figure 14 shows estimates of how increasing the size of the sensor by a factor F affects the low frequency sensitivity of the sensor and the search distance under limiting conditions.

This suggests the use of larger probes particularly in deeper holes where signal levels are low since deep holes are normally drilled to a greater diameter. This specialisation has not occurred except that earlier generation tools were of smaller diameter either 26mm (1in) or 32mm (1.25in). The current models of 3-axis EM probes available have all basically the same outer diameter of 38mm (1.5in). These probes are suitable for holes of B or larger. Probes of appreciably larger diameters would likely be limited in use to holes N size or larger.

Figure 14: Effect of probe size increase factor F on the low frequency sensitivity and estimated search distance when low frequency intrinsic noise is the limiting factor. The search distance is to the nearest conductor edge. A conductor near the detectability limit would be detectable at roughly twice the distance with a sensor scaled by a factor of two.
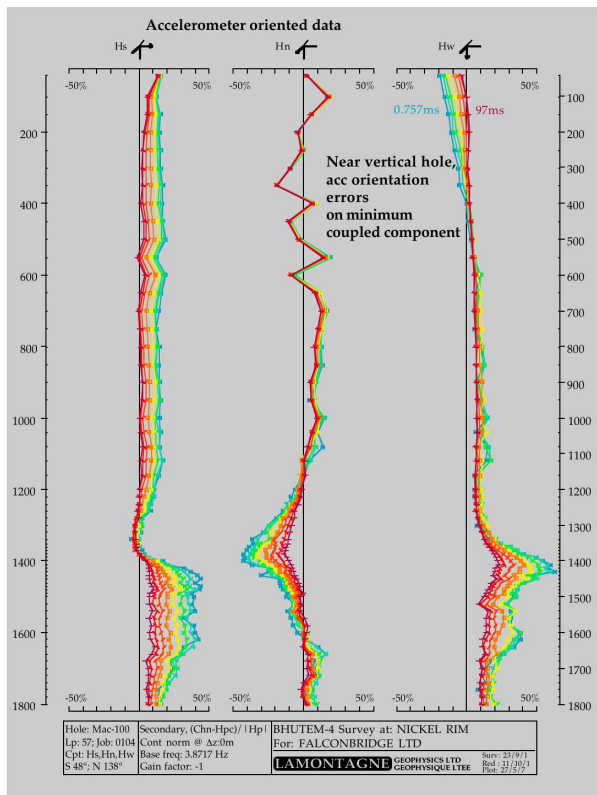
DATA EXAMPLES

BHEM data can range from the simple to the very complex to interpret.

Example 1: Nickel Rim South, simple target shooting

Figure 15 shows an example of a relatively simple data set. These BHUTEM4 data were collected in 2001 at 3.9 Hz as a follow-up of an axial component anomaly obtained in a systematic deep drilling/BHEM program carried out by Falconbridge in the area in the mid-90's. The presentation as shown originally used a drill section (s direction) of 48° and an n azimuth of 138°. The plots show secondary field data obtained

_____

by subtracting the calculated primary field in the measured directions and expressed as a percentage of the calculated primary field amplitude. The axial component data (Hw) show an easily recognisable off-hole anomaly which includes a well defined peak at 1400m depth and a broader anomaly at 1600m.
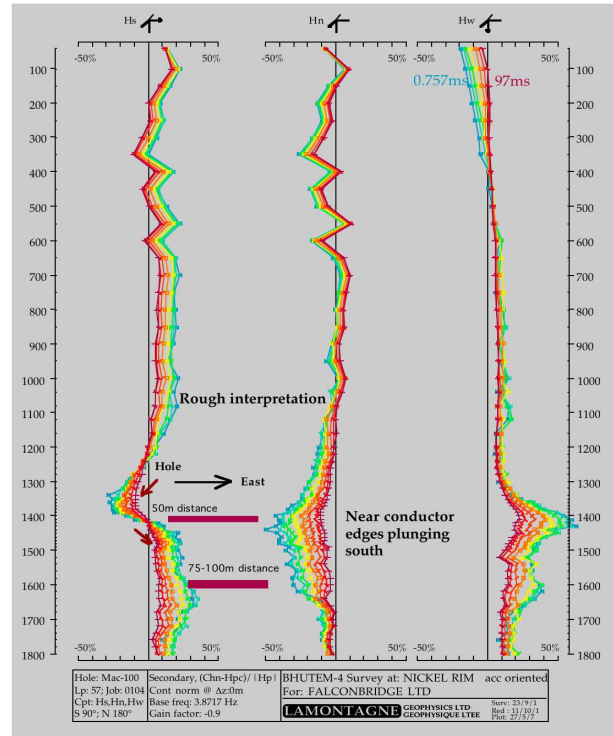
The transverse (Hs and Hn) responses were of shapes that were combinations of symmetric and antisymmetric anomaly shapes. A presentation with the s direction rotated to 90° (n to 180°) (Figure 16) gives simpler looking anomalies with a well defined cross-over corresponding to the Hw anomaly peak which is classical for an off-edge conductor. The arrows drawn on the Hs axis are depicting the direction of the secondary field inferred from the Hw and Hs data. They show the inferred direction of the conductor, to the right of the plot, in the s direction. We also note a broader response gradient corresponding to the 1600m axial anomaly, also interpreted to be east of the hole. A rough interpretation is sketched on the plot. The Hn response has a shape similar to the Hw anomaly but opposite polarity, an indication that the near edge is plunging relative to the hole in the n direction which is to the south.
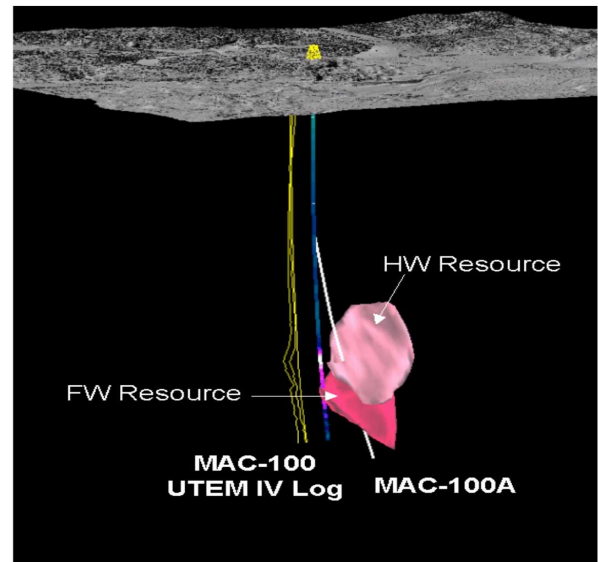

Figure 15: 3-axis data at Mac-100, South Nickel Rim. The minimum coupled component Hn is affected by orientation errors in near vertical part of hole. The Hs and Hn anomalies have a combination of symmetric and anti-symmetric anomaly shapes.

This simple interpretation was done after the fact to illustrate the process. The original interpretation was actually done by Falconbridge geophysicists, with similar conclusions as they drilled a branch Mac100A 100 and 150m east of the original hole at the depths of interest. This hole intersected two main zones of sulphides (Figure 17). This was the discovery hole for

Nickel Rim South deposits. The anomaly at 1400m depth turned out to be due to a contact deposit and the one at 1600m depth to a footwall deposit.

Figure 16: Axis s oriented to the East such that the Hs anomaly is mainly anti-symmetric. Directions of fields indicate that the conductor is east of the hole. The anomalies indicate a much more complex conductive system than the rough interpretation depicted.
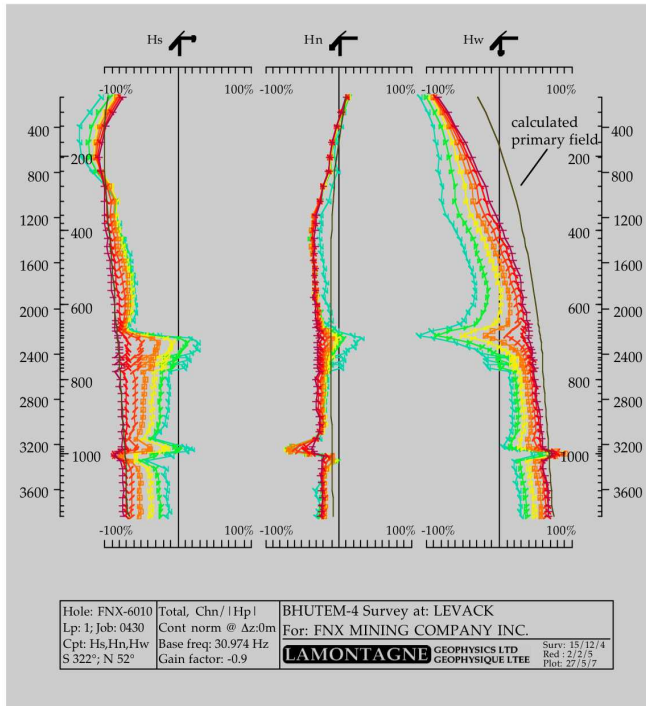

Figure 17: Holes Mac-100/Mac-100A and the Nickel Rim South deposits as presently defined by drilling (courtesy of Xstrata/Falconbridge).

Example 2: Levack Footwall deposit, exploration in a complex conductive environment
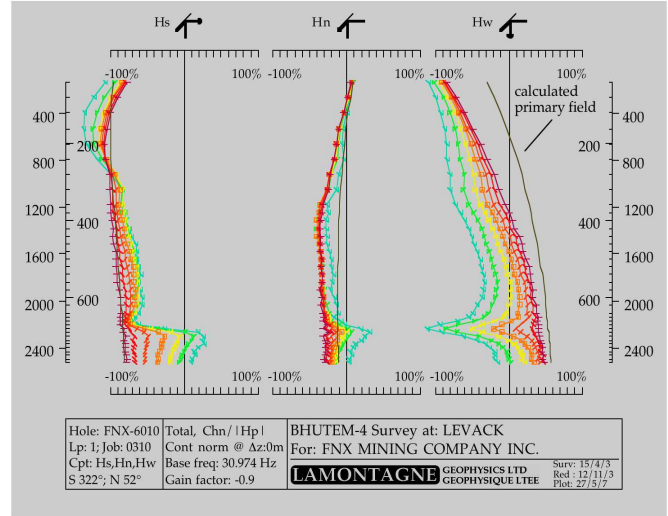
Simple anomaly detection is a relatively rare occurrence in BHEM exploration. In many cases, BHEM measurements are used to try and find new targets among interfering conductors. This was the case for the deep exploration program leading to the discovery of FNX's Levack Footwall deposit.

Figures 18 shows some of the BHUTEM4 results measured with the best coupled of two loops in a routine BHUTEM in April 2003 in hole FNX6010 drilled to 780m depth. There was an obvious narrow in-hole zone at 670m depth and a longer wavelength response due to the known mineralisation around Levack Mine and mining infrastructure. The main question at the time was whether the hole was through the overall mineralised system. Since there was no clear fall-off in the responses near the bottom of the hole, the answer to this was simply no.
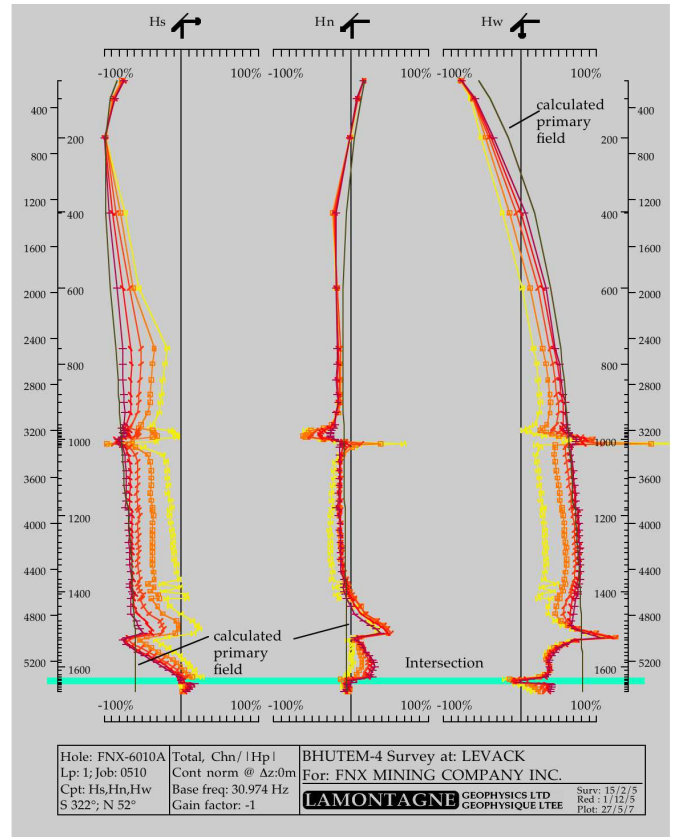
The hole was later re-occupied and deepened to 1170m. Figure 19 show the data obtained with the same loop. A new small very narrow off-hole anomaly was found at 1000m depth. The same question was asked again, and the answer was the same no again. So the hole was deepened again. The hole intersected massive sulphide zones with high metal grades at depths from 1630m to 1660m near the depth limit of the drill. This was the Levack Footwall discovery. The hole was stopped at 1670m and resurveyed with BHEM again (Figure 20). This profile shows a near hole off-hole response in addition to the in-hole response at the intersected zones.
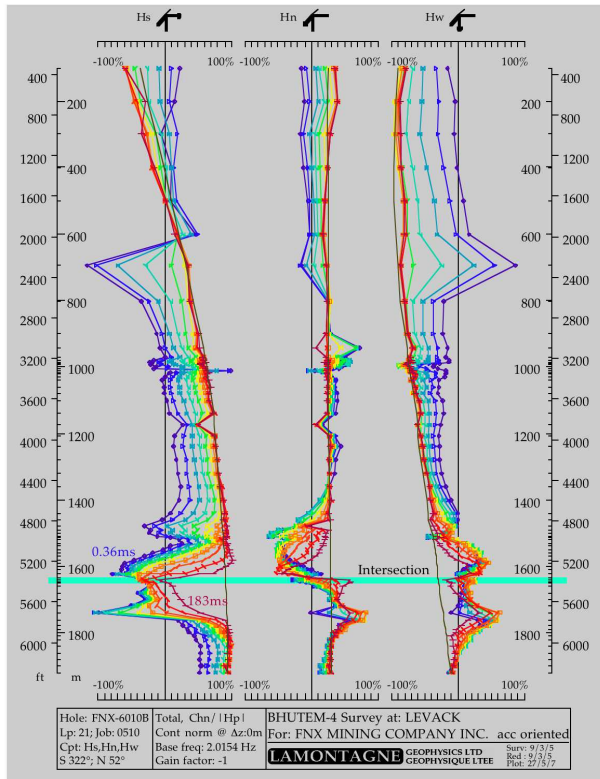

Figure 18: Total field data in hole FNX2010 to original depth of 780m. The data near the top of the hole are affected by the Levack mine infrastructure and geometrical errors. The response is anomalous to the hole bottom.
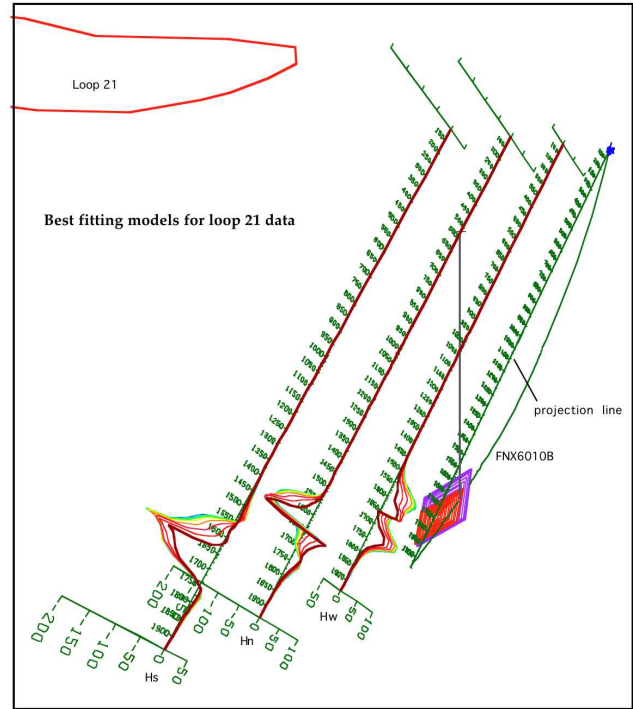

Figure 19: Total field data in hole FNX2010 to deepened depth of 1180m. The bottom of the hole is still in anomalous ground.

Figure 20: Late channel total field data of 31Hz survey with original loop in hole FNX6010 temporarily stopped at 1670m depth. The main intersection anomaly is at 1640m depth. The response is still highly anomalous at the hole bottom.

The hole was then deepened with a larger drill to 1880m and resurveyed again. Figure 21 shows the data obtained at 2Hz base frequency with one loop positioned to well couple with the intersected target and couple less to the main background response. The in-hole zones are much more obvious with this loop, producing anomalies of simpler shape with very long decay. The response of the late channels was modeled with MultiLoop (Figure 22) as a near edge intersection half-way down the depth extent of the conductor, leading one to expect wider intersection towards the conductor centre to the south-west as confirmed by later follow-up hole FNX6045 drilled 70m to the southwest (Figure 23).
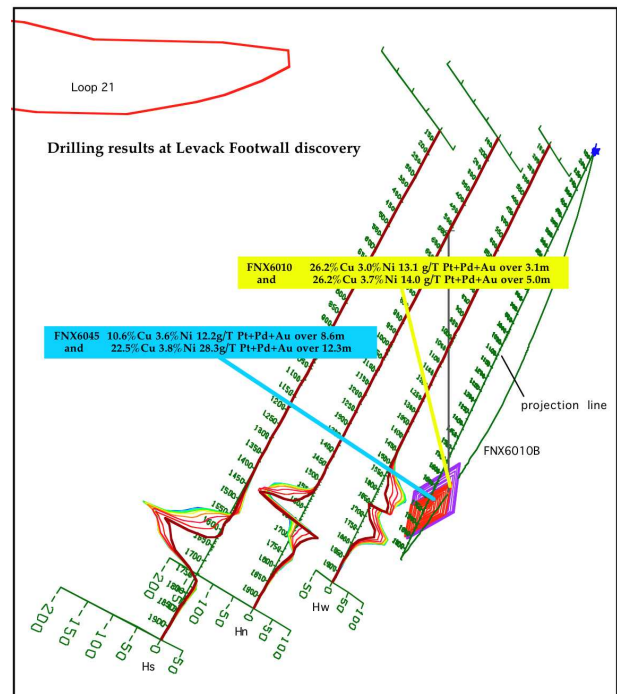
In summary this hole was deepened three times, and eight passes of BHEM measurements made at four hole depths, with two loops and frequencies over two years. The exploration in this hole is a good example of a mineral discovery in a near mine environment where geological insight, BHEM, and perseverance are the essential ingredients for success.

Figure 21: 2 Hz data in hole FNX6010B at final hole depth. Data are in 3-axis 10 channel total field format with calculated primary fields curves in black.

Figure 22: MultiLoop modeling of 2Hz data from loop 21. Plunging view looking W. The modeled conductor centre is to SW and deeper than the intersection.

Figure 23: The follow-up drilling results (blue) showed a wider higher grade intersection than that of the original hole (yellow).

BHEM DATA INTERPRETATION

The interpretation of BHEM data has evolved from being based mainly on type curves and rules of thumb to increasing reliance on software tools.

From a purely geophysical point of view, the main steps in BHEM interpretations are:

1- Anomaly recognition: based on type curves or prior experience.
2- Location of off-hole conductor nearest edge or in-hole conductor centre: based on type curves or sketch of field vectors as in example 1.
3- Rough conductor size and conductance: based on anomaly width and amplitude with the use of templates and response curves.
4- More detailed estimate of conductor size, attitude, and shape: iterative modeling using plate modeling software starting with rough model such as the in-hole example 2. The modelling tools used in this process include Multiloop and Maxwell.
5- Complex responses: use of more advanced modelling tools.

Much of the every day interpretation involves only the first two or three steps but complex responses can warrant a much greater interpretation effort. The main commercially available modelling tools used commonly in BHEM interpretation are mainly approximate plate solutions such as MultiLoop 2 and Maxwell or an approximate 3D modelling tool such as Emigma. MutliLoop 3 uses an extension of the plate formulation to model curved, and connected sheet conductors with electrical connections (Walker and Lamontagne, 2006).
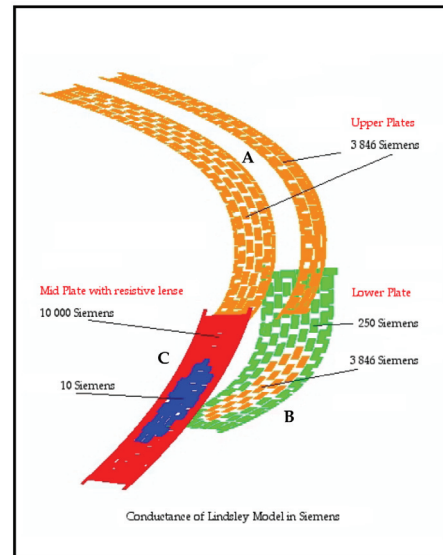
The recent and current developments in BHEM interpretation techniques are on two main fronts. One is the development of tools for the integration of geological and geophysical data and the other the development of more advanced EM modeling tools.

Computer assisted BHEM data management and interpretation has become an important part of its successful application to near mine environments where large volumes of geophysical and geological data must be reconciled (Polzer, 2007).
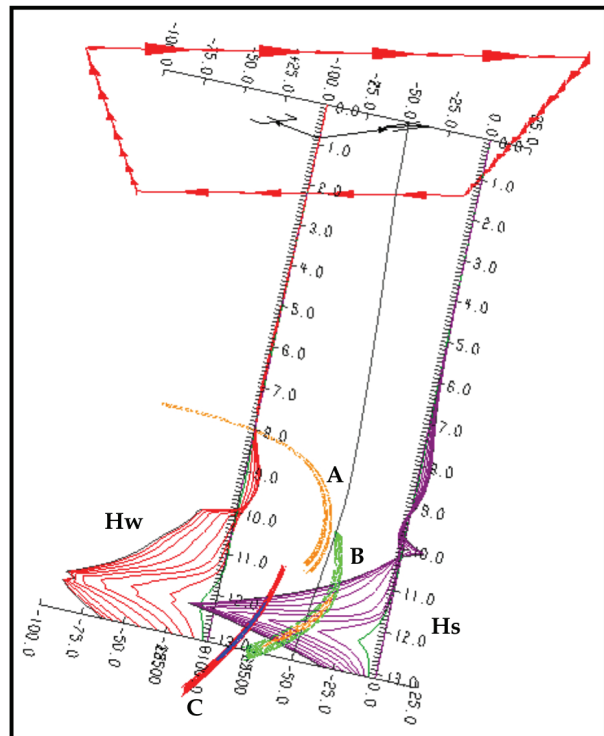
The development of more advanced 3D modelling tools has continued but these have so far had little impact in BHEM interpretation, in part because of the poor behaviour of numerical solutions at points located near or in conductive structures. The other factor preventing a more extensive use of advanced modelling tools in general is that they require much more time to set up, run the solutions, and iterate to a solution matching the data.

For example, Figure 24 shows the curved variable conductance multi-conductor model arrived at with the curved conductor modeling tool MultiLoop 3 in the interpretation of a complex multi-hole data set at Lindley Mine and Figure 25, the modeling results for two component of one hole obtained. In this modelling effort, the goal was to render the data from five boreholes and try to reconcile the BHEM data with the available geological data with the hope unmasking unknown conductors. This particular modelling project took several weeks of trials and errors before the data were matched satisfactorily. In this

modelling, much of the time was often spent on coming up with a rough "correct" starting model aided by available geological data. Only from this point on could iterative changes be used with some success in fitting the observed data.

Figure 24: Curved variable conductance sheet cond-uctors used in modeling the Lindsley BHEM data.

Figure 25: Example of calculated Hw/Hs responses for one hole and one loop in the Lindsley interpretation study. With these loop and hole locations, conductor C is poorly coupled and A has a gap near the hole, so the complex anomaly shapes are due mainly to curved conductor B which is both in-hole and off-hole.

The next step in BHEM interpretation is probably the development of automatic BHEM interpretation tools. The ultimate interpretation tool of the future for BHEM would be a full 3D inversion of data sets with multiple holes and loop locations making use of available geological constraints. This is a difficult problem because it is hard to reconcile the non-systematic spatial coverage provided by the BHEM data in just a few boreholes and the intricate but very local detail of the geological data that are available through core logs.

CONCLUSIONS

Over the last decade BHEM has become an essential part of mineral exploration. The progress achieved can be measured in the significant improvements in the measurement technology and interpretation tools used. Or it can be measured in terms of the increasing number of mineral discoveries that BHEM measurements have contributed to including the two cases presented here and numerous others (Bengert, 2006; Polzer, 2000; Vowles, 2000).

As alluded to in the introduction, perhaps BHEM's greatest achievement over this period has been the renewed confidence it has given to exploration teams in the look for deeply buried mineral deposits.

ACKNOWLEDGEMENTS

REFERENCES

Bengert, Brian, 2006. Successful Application of Electromagnetics in the Reid Brook Zone: Targeting Economic Needles in a Highly Conductive Haystack: Australian Earth Science Convention, Melbourne, July 2006.

Macnae, J.C., Lamontagne, Y., and West, G.F.,1984, Noise processing techniques of time-domain EM systems: Geophysics, 49, 934-948.

Ravenhurst, W.R., 1998. Step and Impulse Calculations from Pulse-type Time Domain Electromagnetic Data: SEG International Meeting, New Orleans, 1998.

Smith, R.S, and Balch, S.J., 1998. Robust estimation of the in-phase response from impulse response TEM measurements taken during the transmitter switch off and the transmitter off-time: Theory and an example from Voisey's Bay, Labrador, Canada. Geophysics, 65,, 476-481.

Polzer, B., 2007. A new tool for the integration of, vizualisation and processing of exploration data: PDAC 2007, Toronto, Canada.

Polzer, B., 2000. The role of Borehole EM in the Discovery and Definition of the Kelly Lake Cu-Ni Deposit, Sudbury, Canada: SEG International Meeting, Calgary 2000.

Vowles, A.K., 2000. A case history of the discovery of the Chisel North zinc/copper deposit: SEG International Meeting, Calgary 2000.

Walker, P., and Lamontagne Y., 2007. Electromagnetic interpretation in complex geological environments: SEG International Meeting, New Orleans, 2006.